Materials Physics and Mechanics 47 (2021) 237-244 Received: February 5, 2021

MOLECULAR DYNAMICS STUDY OF STRESS-STRAIN CURVES FOR γ-Fe AND HADFIELD STEEL IDEAL CRYSTALS AT SHEAR ALONG THE <111> DIRECTION

G.M. Poletaev[1], R.Y. Rakitin[2]

[1]Altai State Technical University, Lenin Str. 46, 656038 Barnaul, Russia

[2]Altai State University, Lenin Str. 61, 656049 Barnaul, Russia

*e-mail: gmpoletaev@mail.ru

Abstract. The molecular dynamics method was used to simulate the shear along the <111> direction in Hadfield steel and a pure fcc Fe crystal. The stress-strain curves are obtained depending on the shear rate, the size of the computational cell, and temperature. It is shown that the shear rate in the range of 10–100 m/s has little effect on the theoretical strength at a constant temperature. With increasing temperature, the slope of the stress-strain dependences in the elastic region decreased, which is due to the temperature dependence of the elastic moduli. In addition, the temperature significantly influenced the theoretical strength – with an increase in temperature, plastic deformation began in ideal crystals at lower deformation values. Moreover, this dependence was more pronounced for a pure fcc Fe crystal than for Hadfield steel, which initially had structural imperfections caused by the presence of impurities that facilitate the initiation of plastic shears in a pure crystal. In this regard, at medium and low temperatures, the theoretical strength of pure iron was higher than that of steel. But at high temperatures (above 1200 K), its values for both materials became almost the same.

Keywords: molecular dynamics, theoretical strength, stress-strain curve, Hadfield steel

1. Introduction

Hadfield steel, due to its excellent ability to work hardening [1,2], has great practical importance and a long history of research into its unique properties. At the same time, today there are very few works devoted to modeling its atomic structure and the processes occurring in it under conditions of deformation at the atomic level, which is due, in particular, to the complexity of modeling such multicomponent systems. Currently, there are a number of issues related to the mechanisms of plastic deformation at the atomic level in steels and which can be solved mainly by computer simulation methods. Such questions include, for example, the features of the formation and propagation of dislocations depending on various factors, the mechanisms of interaction with each other, grain boundaries, twins, and other defects.

The presence of impurity atoms in the metal lattice, as is the case in steel, complicates the process of dislocation motion. Impurity atoms of light elements (in this case, it is mainly carbon), even at low concentrations, strongly affect the mechanical properties of metals and alloys. Interacting with dislocations and preventing their movement, impurities lead to an increase in the strength, hardness, and frictional properties of metals, together, as a rule, with brittleness [3-5]. The energy of their bonding with dislocations is positive, as a result of which they tend to be fixed on dislocations and form the so-called Cottrell atmosphere [6-8]. In

http://dx.doi.org/10.18149/MPM.4722021_6

addition to the Cottrell mechanism, impurities, like most other defects, are effective stoppers for moving dislocations, which was confirmed not only by experimental studies but also by computer simulations [9,10]. In [9], for example, using molecular dynamics, it was found that the critical stress at which a dislocation begins to slip in α-Fe increases with an increase in the concentration of carbon atoms. In [10], also carried out using the method of molecular dynamics, it was shown that with an increase in the carbon concentration, the slip rate of dislocations in iron decreases. In metals with an fcc lattice, in addition to the aforementioned mechanisms of deceleration of dislocations by impurities, the Suzuki mechanism is also connected – the pinning of impurity atoms at a stacking fault between partial dislocations [3,4].

This work is devoted to the study of stress-strain curves depending on various factors for γ-Fe and Hadfield steel ideal crystals at shear along the <111> direction. Separate consideration of the behavior of an ideal crystal of fcc iron is associated with the desire to highlight the role of impurities in Hadfield steel – manganese and carbon. It is known that in crystals with an fcc lattice, the {111}<110> slip system is predominant [11,12]. The choice of the <111> direction of shear is due to two reasons. First, in this case, two slip systems are involved, and it is of interest to study the joint operation and interaction of dislocations of two different systems. Second, this model is supposed to be used to further study the plastic deformation of samples containing a system of parallel twins oriented perpendicular to the shear direction.

2. Description of the model

Hadfield steel, as is known, is a multi-component system and, in addition to classical iron, manganese, and carbon, may contain some other alloying elements [1,2]. In this study, we limited to a system that included three elements: γ-Fe as a matrix, Mn, and C.

To describe the Fe-Fe interactions in austenite matrix, it was used Lau EAM potential [13], which reproduces well the structural, energy, and elastic characteristics of austenite. These are classic EAM potentials, where the energy of the *i*-th atom is calculated as the sum of the pair and multiparticle components:

$$E_{\alpha,i} = -A_\alpha\sqrt{\sum_{j\neq i}\rho_{\beta\alpha}(r_{ij})} + \frac{1}{2}\sum_{j\neq i}\phi_{\beta\alpha}(r_{ij}),$$
$$\rho_{\beta\alpha}(r_{ij}) = t_1(r - r_{c,\rho})^2 + t_2(r - r_{c,\rho})^3, \qquad r \le r_{c,\rho}\ , \tag{1}$$
$$\phi_{\beta\alpha}(r_{ij}) = (r - r_{c,\phi})^2(k_1 + k_2 r + k_3 r^2), \qquad r \le r_{c,\phi}\ .$$

We drew attention to this potential primarily because it was tested in detail in [14] when describing the structural, energy, and elastic characteristics of austenite.

For all other five interactions, Morse potentials are proposed, the parameters of which were found from various experimental characteristics, in particular, the energy of dissolution and the energy of migration of an impurity in fcc iron crystal, the radius of atoms, their electronegativity, mutual binding energy, etc. The Morse potential is pair, but it is often used in molecular dynamics calculations, including the description of interatomic interactions in metals. Pair potentials are relatively often used by various researchers to describe interatomic interactions in metal-impurity systems [15-21]. The Morse potential determines the interaction energy of a pair of atoms located at a distance *r* from each other:

$$\varphi(r) = D\beta e^{-\alpha r}(\beta e^{-\alpha r} - 2)\ , \tag{2}$$

where α, β, D are the potential parameters.

All Morse potentials were found for a cutoff radius of 4.7 Å, i.e. taking into account the three coordination spheres in fcc Fe. Considering a larger number, for example, of five spheres, as we did, for example, in [20-22], leads to a significant slowdown in the counting

speed compared to taking into account three spheres, but at the same time, to a relatively small increase in accuracy, not exceeding a few percent.

Table 3. Parameters of Morse potentials for the considered interactions

Bond	α (A^{o-1})	β	D eV)
Fe-C	1.82	41	0.41
C-C	1.97	50	0.65
Mn-Mn	1.321	39.792	0.373
Mn-Fe	1.306	38.030	0.413
Mn-C	1.87	43	0.777

The standard ratio of components was used: Mn – 13 wt.% and C – 1.2 wt.% (12.63 at.% и 5.33 at.%, respectively) [1,2]. Mn atoms were introduced into fcc iron lattice randomly by replacing Fe atoms. The sizes of Fe and Mn atoms are very close, therefore, Mn atoms create small distortions in the iron lattice. But at the same time, Mn atoms have a much stronger bond with carbon atoms. The binding energy of Mn and C atoms in austenite lattice is very high – 0.35 eV, according to [23], which is approximately the same as, for example, the binding energy of carbon atoms with vacancies (0.37-0.41 eV [24]). Both of them are a kind of effective “traps” for impurity carbon atoms, not allowing them, in particular, to form clusters on dislocations and grain boundaries. This has a positive effect on the mechanical properties of steel, since these accumulations of carbon atoms, as a rule, lead to the development of negative phenomena such as embrittlement and aging [6].

In fcc, hcp, and bcc lattices of metals, impurity atoms of light elements (such as C, N, O, etc.), according to numerous studies, occupy octahedral voids, in which, as is known, the largest amount of free volume of the crystal lattice is concentrated [3,4]. In this connection, carbon atoms were introduced into the octahedral voids closest to Mn atoms. The number of carbon atoms corresponded to a given concentration. The choice of Mn atoms near which C atoms were introduced, as well as the selection of one of the neighboring octahedral voids, were made randomly.

In pure fcc iron, which was considered in this work for comparison with Hadfield steel, the type of the crystal lattice remained constant over the entire temperature range; the polymorphic transformation was not taken into account in this work. As mentioned above, pure austenite was considered to determine the contribution of Mn and C impurities in the processes under study.

The computational cell of fcc Fe contained 122760 atoms (of Hadfield steel – 130173 atoms) and had a length of 27.2 nm, a height of 20.3 nm, and a thickness of 2.5 nm. Along the X and Y axes (Fig. 1), an endless repetition of the structure was simulated, i.e. periodic boundary conditions were imposed. The shear in the model was initiated by the displacement of atoms in the upper and lower regions highlighted by light gray in Fig. 1 in opposite directions along and against the Y-axis (the [111] direction). The areas in the upper and lower parts of the cell in the course of the computer experiment moved as a whole. The movement of the remaining atoms in the computational cell was not limited; it was described by the classical equations of motion of Newton.

The strain rate usually varies from 10^{-5} to 10^{5} s^{-1} [25]. At rates above 10^{3} s^{-1}, deformation is usually considered high-rate, which is characterized by a significant increase in strength and, as a rule, a brittle nature of fracture [25]. Due to the peculiarities of the molecular dynamics method, the deformation rate in the model can be set in the range 10^{8}-10^{11} s^{-1}. However, this does not mean that the imaginary "clamps" on the sample move at a tremendous speed, their speed is quite ordinary: 10^{0}-10^{3} m/s. Such a high rate of

deformation is caused to the very small size of the sample (as a rule, only a few tens of nm), due to which the rate of change in the relative deformation is relatively high.

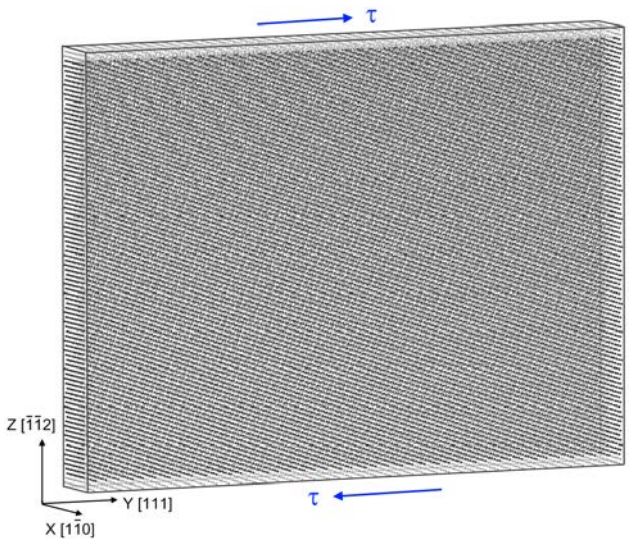

Fig. 1. Computational cell for modeling shear along the [111] direction (Y axis)

The time integration step in the molecular dynamics method was 2 fs. The temperature in the model was set through the initial velocities of the atoms according to the Maxwell-Boltzmann distribution, taking into account the change in the lattice parameter due to thermal expansion. To keep the temperature constant during the simulation, a Nose-Hoover thermostat was used.

3. Results and discussion

In the present work, we investigated the effect of strain rate, computational cell size, and temperature on stress-strain curves. Figure 2a shows stress-strain plots obtained at shear rates (displacements relative to each other of the upper and lower regions of the computational cell) of 10, 20, 50, and 100 m/s.

The theoretical shear strength of metal crystals is known to be very high and can reach more than ten GPa [26]. The introduction of just one dislocation into a pure crystal in the molecular dynamics model reduces the strength to several hundred MPa [27]. As seen from Fig. 2, plastic deformation in a pure fcc iron crystal at a temperature of 300 K began only when shear deformation along the [111] direction was more than 12% and shear stress of 9 GPa. It should also be emphasized that the crystal was initially not only ideal but also did not contain any sources of dislocation formation, even a free surface. In this regard, the intervals of elastic deformation on the graphs were relatively large.

The slope of the stress-strain dependence, as can be seen, does not change with increasing strain rate. The slope is essentially the shear modulus in Hooke's equation, i.e. the resistance of the crystal to elastic deformation does not change with an increase in the rate of this deformation. However, at the same time, as seen in Fig. 2a, the value of deformation changes slightly at which irreversible plastic shears begin in the computational cell. The crystal response is, as it were, lagged at very high shear rates. Because of this "lag" connected with the finite speed of propagation of elastic waves, the stepped nature of the stress-strain dependence at high strain rates is associated. Moreover, the higher the deformation rate, the greater these steps (in Fig. 2a, for example, steps for speeds of 50 and 100 m/s are clearly visible).

The results obtained at rates of 10 and 20 m/s were almost the same. However, it was decided to use a shear rate of 10 m/s for further research. In units of relative deformation, this is $4.9 \cdot 10^8$ s^{-1}.

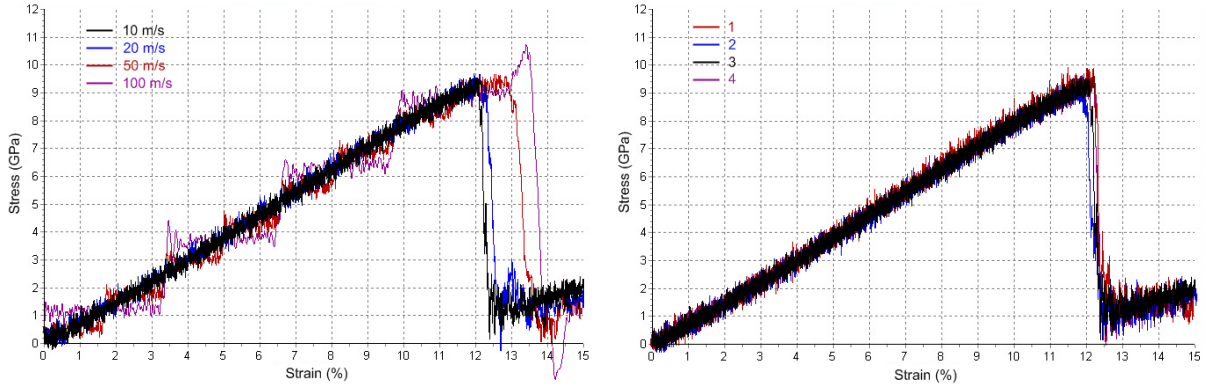

a) b)

Fig. 2. Stress-strain curves for a pure fcc iron crystal at a temperature of 300 K: a) at different shear rates along the Y axis of 10, 20, 50, and 100 m/s; b) for four sizes of the computational cell at a shear rate of 10 m/s: 1 – 12.4×9.2 nm, 2 – 17.3×12.9 nm, 3 – 22.3×16.8 nm, 4 – 27.2×20.3 nm

The second step was to study the effect of the size of the computational cell on the stress-strain curves. For this, we considered four cells of different sizes along the Y and Z axes: 12.4×9.2 nm, 17.3×12.9 nm, 22.3×16.8 nm, 27.2×20.3 nm. The thickness in all cases was the same – 2.5 nm. According to the results obtained (Fig. 2b), all the considered sizes of the computational cells give identical stress-strain dependences. The differences are completely insignificant and relate mainly to the plastic mode of deformation. In the rest of the computer experiments, we used cells No. 4 – 27.2×20.3 nm.

Figure 3 shows the dependences τ(ε) for an ideal crystal of fcc iron (a) and Hadfield steel (b) at different temperatures. It is known that elastic moduli in a wide temperature range decrease almost linearly with increasing temperature, which is usually associated with thermal expansion [28]. In addition, it can be seen that the temperature significantly affects the probability of dislocation formation and the onset of the plastic phase – with increasing temperature, plastic deformation begins earlier. Moreover, this dependence is quite strong – at a temperature of 100 K, plastic shears in fcc Fe began at a deformation of about 14.5%, and at a temperature of 1200 K – already at 8%. This is most likely explained by the fact that the formation of dislocation is an activation process (i.e. certain finite activation energy is required for the formation of a dislocation), which obeys the classical Arrhenius law, i.e. the probability of dislocation formation is proportional to $exp(-E/kT)$, where E is the activation energy of plastic shear formation in the considered computational cell, k is the Boltzmann constant, and T is the temperature.

The shift of the point of the beginning of the plastic phase with increasing temperature occurs faster in iron than in steel, and at a temperature of 1200 K they almost coincide. At medium and low temperatures, the curves for steel and pure austenite differ greatly – in steel the plastic phase occurs at much lower deformation values than in pure iron. For example, at a temperature of 300 K, dislocations are formed in steel already at a shear of 9%, whereas in fcc iron at 12% (black graphs in Fig. 3). This is explained by the presence of imperfections in the steel, distortions of the crystal lattice, caused by the presence of impurities, which facilitates the initiation of plastic shears, i.e. the formation of dislocations in a pure crystal.

Another noticeable difference between the graphs for iron and steel is that in steel, after the onset of the plastic phase, the stresses remain approximately two times higher than in iron.

As for the similarity, it is the same slope of the dependencies in the elastic region for steel and iron at the same temperatures. This is due to the fact that, despite significant differences in the strength of iron and steel, their elastic characteristics, as a rule, are very close [29].

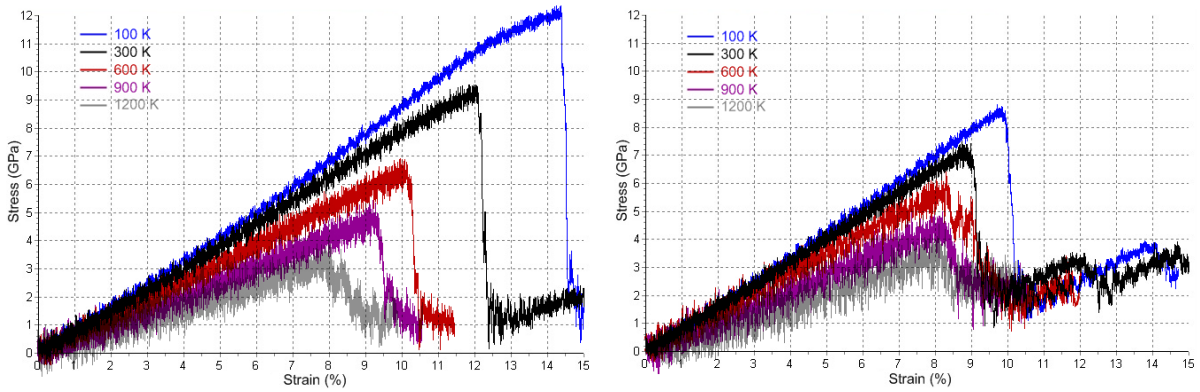

a) b)

Fig. 3. The dependences τ(ε) for an ideal crystal of fcc iron (a) and Hadfield steel (b) at different temperatures

Figure 4 shows examples of plastic shears in the computational cells of fcc iron and Hadfield steel deformed by 15%. For this type of loading, shears appear in two planes of the (111) type. The effect of impurities in steel is clearly seen: despite the fact that plastic shears are initiated earlier in steel than in pure iron dislocations propagate and develop much weaker, slip bands are smaller and their number is fewer (Fig. 4b). In pure iron, the process of formation of deformation twins was also more intense – wide vertical dark bands in Fig. 4a.

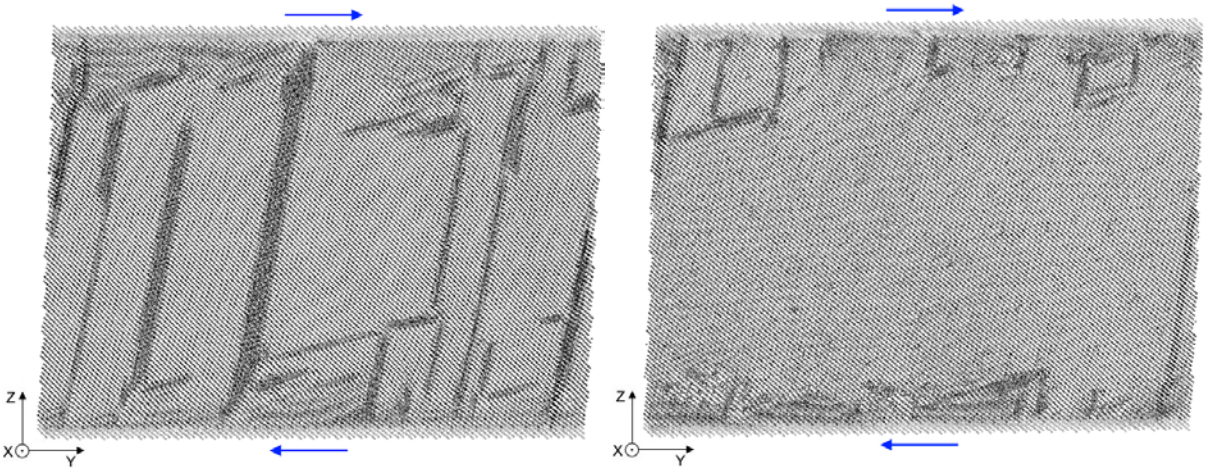

a) b)

Fig. 4. Dislocations in pure fcc Fe (a) and Hadfield steel (b) formed as a result of shear along the Y axis [111] by 15%. The computational cell is rotated so that the slip bands are better visible

4. Conclusion

The molecular dynamics method was used to simulate the shear along the <111> direction in Hadfield steel and a pure fcc Fe crystal. The stress-strain curves are obtained depending on the shear rate, the size of the computational cell, and temperature. It is shown that the shear rate in the considered range of 10–100 m/s has little effect on the theoretical strength at a constant temperature. One should, of course, expect a change in the theoretical strength at high strain rates, close in order to the speed of sound in the metal.

With increasing temperature, the slope of the stress-strain dependences in the elastic region decreased, which is due to the temperature dependence of the elastic moduli. In addition, the temperature significantly influenced the theoretical strength – with an increase in temperature, plastic deformation began in ideal crystals at lower deformation values. Moreover, this dependence was more pronounced for a pure fcc Fe crystal than for Hadfield steel, which initially had structural imperfections caused by the presence of impurities that facilitate the initiation of plastic shears in a pure crystal. In this regard, at medium and low temperatures, the theoretical strength of pure iron was higher than that of steel. But at high temperatures (above 1200 K), its values for both materials became almost the same.

For the considered type of loading, shear along the <111> direction, dislocations arose in two slip systems. Moreover, in steel, due to the action of impurities, plastic shears occurred at lower deformation values than in pure iron, but the dislocations propagated and developed much weaker, slip bands were noticeably smaller, and their number was also smaller.

Acknowledgements. *No external funding was received for this study.*

References

[1] Zhang FC, Lv B, Wang TS, Zheng CL, Zhang M, Luo HH, Liu H, Xu AY. Explosion hardening of Hadfield steel crossing. *Materials Science and Technology*. 2010;26(2): 223-229.

[2] Chen C, Lv B, Ma H, Sun D, Zhang F. Wear behavior and the corresponding work hardening characteristics of Hadfield steel. *Tribology International.* 2018;121: 389-399.

[3] Goldschmidt HJ. *Interstitial Alloys*. London: Butterworths; 1967.

[4] Toth LE. *Transition metal carbides and nitrides.* New York: Academic Press; 1971.

[5] Poletaev GM, Zorya IV. Effect of light element impurities on the edge dislocation glide in nickel and silver: molecular dynamics simulation. *Journal of Experimental and Theoretical Physics.* 2020;131(3): 432-436.

[6] Clouet E, Garruchet S, Nguyen H, Perez M, Becquart CS. Dislocation interaction with C in α-Fe: A comparison between atomic simulations and elasticity theory. *Acta Materialia.* 2008;56: 3450-3460.

[7] Veiga RGA, Goldenstein H, Perez M, Becquart CS. Monte Carlo and molecular dynamics simulations of screw dislocation locking by Cottrell atmospheres in low carbon Fe–C alloys. *Scripta Materialia.* 2015;108: 19-22.

[8] Poletaev GM, Zorya IV, Rakitin RY, Glubokova LG. The binding energy of impurity atoms C, N, O with edge dislocations and the energy of their migration along dislocation core in Ni, Ag, Al. *Materials Physics and Mechanics.* 2020;44(3): 404-410.

[9] Granberg F, Terentyev D, Nordlund K. Interaction of dislocations with carbides in BCC Fe studied by molecular dynamics. *Journal of Nuclear Materials.* 2015;460: 23-29.

[10] Njoroge KD, Rading GO, Kihiu JM, Witcomb MJ, Cornish LA. The impact of interstitial carbon on dislocation motion in the alpha-Fe lattice. *International Journal of Computational Engineering Research.* 2014;4: 5-9.

[11] Friedel J. *Dislocations*. Oxford: Pergamon press; 1964.

[12] Hirth JP, Lothe J. *Theory of Dislocations.* 2nd ed. NY: Wiley; 1982.

[13] Lau TT, Forst CJ, Lin X, Gale JD, Yip S, Van Vliet KJ. Many-body potential for point defect clusters in Fe-C alloys. *Physical Review Letters.* 2007;98: 215501.

[14] Oila A, Bull SJ. Atomistic simulation of Fe–C austenite. *Computational Materials Science.* 2009;45(2): 235-239.

[15] Xie JY, Chen NX, Shen J, Teng L, Seetharaman S. Atomistic study on the structure and thermodynamic properties of Cr_7C_3, Mn_7C_3, Fe_7C_3. *Acta Materialia.* 2005;53(9): 2727-2732.

[16] Ruda M, Farkas D, Abriata J. Interatomic potentials for carbon interstitials in metals and intermetallics. *Scripta Materialia.* 2002;46: 349-355.
[17] Vashishta P, Kalia RK, Nakano A, Rino JP. Interaction potentials for alumina and molecular dynamics simulations of amorphous and liquid alumina. *Journal of Applied Physics.* 2008;103(8): 083504.
[18] Liu SJ, Shi SQ, Huang H, Woo CH. Interatomic potentials and atomistic calculations of some metal hydride systems. *Journal of Alloys and Compounds.* 2002;330-332: 64-69.
[19] San Miguel MA, Sanz JF. Molecular-dynamics simulations of liquid aluminum oxide. *Physical Review B.* 1998;58(5): 2369-2371.
[20] Poletaev GM, Zorya IV, Rakitin RY, Iliina MA. Interatomic potentials for describing impurity atoms of light elements in fcc metals. *Materials Physics and Mechanics*. 2019;42(4): 380-388.
[21] Poletaev GM, Zorya IV. Influence of light impurities on the crystal-melt interface velocity in Ni and Ag. Molecular dynamics simulation. *Technical Physics Letters.* 2020;46: 575-578.
[22] Poletaev GM, Novoselova DV, Zorya IV, Starostenkov MD. Formation of the excess free volume in triple junctions during nickel crystallization. *Physics of the Solid State.* 2018;60: 847-851.
[23] Massardier V, Le Patezour E, Soler M, Merlin J. Mn-C interaction in Fe-C-Mn steels: study by thermoelectric power and internal friction. *Metallurgical and Materials Transactions A.* 2005;36A: 1745-1755.
[24] Slane JA, Wolverton C, Gibala R. Carbon-vacancy interactions in austenitic alloys. *Materials Science and Engineering A.* 2004;370(1-2): 67-72.
[25] Evstifeev AD, Gruzdkov AA, Petrov YV. Dependence of the type of fracture on temperature and strain rate. *Technical Physics. The Russian Journal of Applied Physics.* 2013;58(7): 989-993.
[26] Bukreeva KA, Iskandarov AM, Dmitriev SV, Mulyukov RR, Umeno Y. Theoretical shear strength of fcc and hcp metals. *Physics of the Solid State.* 2014;56: 423-428.
[27] Krasnikov VS, Kuksin AY, Mayer AE, Yanilkin AV. Plastic deformation under high-rate loading: the multiscale approach. *Physics of the Solid State.* 2010;52: 1386-1396.
[28] Shtremel MA. *Strength of alloys. P.1. Lattice defects.* Moscow: Metallurgiya; 1982. (In Russian)
[29] Lide DR. (Ed.) *CRC Handbook of Chemistry and Physics* Boca Raton: CRC Press; 2005.